

# Stochastic Wave-Function Method versus Density Matrix: a Numerical Comparison

Heinz-Peter Breuer, Wolfgang Huber, and Francesco Petruccione

*Albert-Ludwigs-Universität, Fakultät für Physik,*

*Hermann-Herder-Straße 3, D-79104 Freiburg im Breisgau, Federal Republic of Germany*

(April 25, 1997)

Numerical investigations of open quantum systems, which are widely performed in such fields as photochemistry, quantum optics and nuclear magnetic resonance, can, in the Markovian regime, be based either on the master equation for the reduced density operator or on a stochastic process in the Hilbert space of the reduced system. It is shown that the CPU time consumptions of the two methods depend on the system size  $N$  as  $N^{\alpha+1}$  and as  $R(N) N^\alpha$ , respectively. The exponent  $\alpha$  is characteristic of the specific system.  $R(N)$  is the number of process realizations generated in the simulation and is defined by prescribing the tolerable statistical error of the result. Since  $R(N)$  is a non-increasing function of  $N$ , the stochastic method is found to be always faster for large systems. This is demonstrated for the example of the dissipative Morse oscillator excited by an intense short laser pulse.

02.70.Lq, 33.80.-b, 42.50.Lc

---

Corresponding author:

W. Huber, email: [Wolfgang.Huber@physik.uni-freiburg.de](mailto:Wolfgang.Huber@physik.uni-freiburg.de), Fax: (+49) 761 - 203 5967

## I. INTRODUCTION

During recent years, the Monte Carlo wave-function method has been proposed for investigating dissipative quantum systems [1–5]. Besides providing insight into statistical properties which are not revealed by the density operator master equation approach, the Monte Carlo wave-function method has been designed as an efficient computational tool for the treatment of large systems as encountered, for instance, in photochemistry [6] and laser cooling [7]. For a system with  $N$  states, the density matrix treatment requires simultaneous solution of  $O(N^2)$  equations, while the stochastic wave-function approach involves the time evolution of no more than  $N$  variables.

As with any Monte Carlo method, the results are subject to a statistical error. This error is related to the number of realizations of stochastic wave-functions that are generated in the simulation. The total CPU time required by the Monte Carlo wave-function method thus depends on the desired accuracy.

This article presents a systematic analysis of the time consumption of the Monte Carlo wave-function method and compares it with that of the numerical solution of the corresponding density matrix equation. The main interest lies on the dependency of the time-consumption on the system size  $N$ . It will be shown that for sufficiently large  $N$  and for any prescribed, fixed statistical error the stochastic wave-function method is always faster than the integration of the corresponding density matrix equation.

The article is structured as follows. Section II contains a general, quantitative formulation of the relations between CPU time consumption, system size and statistical errors. In Section III these general considerations are illustrated with an explicit example. The example is non-trivial and concerns the excitation of molecular vibrations by short laser pulses in a dissipative environment. The results are summarized in Section IV.

## II. GENERAL CONSIDERATIONS ON NUMERICAL PERFORMANCE

### A. Reduced density operator and stochastic wave-function method

Dissipation in a quantum system arises when the system is coupled to environmental degrees of freedom whose dynamics need not or cannot be described explicitly. The environment is then taken into account by introducing suitable dissipative terms in the system's dynamic equations. The typical situation encountered, for instance, in quantum optics and laser physics is a bound system, e. g., an atom or molecule, coupled to an environment which consists of a continuum of electromagnetic field modes.

One fashion to formulate the dynamics of the open quantum system employs the reduced density operator,

which is obtained from the density operator of the total system by tracing over the variables of the environment. In order to derive a closed equation for the reduced density operator, various approximation techniques are known [8,9]. The most famous of these is the Markov approximation which yields under certain additional assumptions the so-called quantum optical Markovian master equation [10–13], that is a linear differential equation for the density operator  $\rho$

$$\frac{d\rho}{dt} = -\frac{i}{\hbar} [H_S, \rho] + \sum_i \gamma_i \left( A_i \rho A_i^\dagger - \frac{1}{2} A_i^\dagger A_i \rho - \frac{1}{2} \rho A_i^\dagger A_i \right). \quad (1)$$

The Hamiltonian  $H_S$  describes the coherent part of the dynamics. The dissipation is represented by the operators  $A_i$  and the rates  $\gamma_i$ . The form of Eq. (1) guarantees that the properties of a density operator, i. e., Hermiticity, normalization and semi-positivity, are preserved. In principle, the numerical solution of Eq. (1) is straightforward. Introducing a basis, the resulting set of linear coupled differential equations for the matrix elements of  $\rho$  can be solved by a standard numerical integration routine. However, if the dimension of the matrix is large, CPU time and memory requirements impose limits on the calculations.

In recent years several stochastic wave-function methods have been developed for the description of open quantum systems [1–4]. The essence of these methods is the use of ensembles of pure states. Instead of an equation of motion for the density matrix, the dynamics is formulated in terms of a stochastic process in the system's Hilbert space. Again, a Markov approximation can be made, and the process is then found to be a piecewise-deterministic Markov process. Individual realizations of the process consist of intervals of deterministic time evolution interrupted by a discrete set of jumps. The process can be characterized by the density  $T[\psi, t | \tilde{\psi}, t_0]$  of the conditional transition probability to find the system in state  $\psi$  at time  $t$ , given that it was in state  $\tilde{\psi}$  at time  $t_0$ . Its short time behaviour takes the form [14,15].

$$T[\psi, t + \tau | \psi', t] = (1 - \tau \Gamma[\psi']) \delta \left[ \psi' - \frac{i\tau}{\hbar} G(\psi') - \psi \right] + \tau W[\psi | \psi'] + O(\tau^2). \quad (2)$$

The deterministic part of the process is induced by the non-linear operator  $G$ : as long as no jump occurs, individual realizations evolve according to  $\partial\psi/\partial t = -iG(\psi)/\hbar$ . The stochastic part of the process is described by the transition rate  $W[\psi | \psi']$  of a jump from  $\psi'$  to  $\psi$ . Denoting by  $P[\psi, t]$  the one-time probability density, the ensemble average of the quantum mechanical expectation value  $\langle \psi | B | \psi \rangle$  of an observable  $B$  is defined as [14,16]

$$E_t[B] = \int \langle \psi | B | \psi \rangle P[\psi, t] D\psi D\psi^*, \quad (3)$$

where  $D\psi D\psi^*$  is the volume element in the system's Hilbert space, and the integration extends over the whole space.

The numerical aspect of the stochastic wave-function approach is an algorithm that generates a finite sample of size  $R$  of independent realizations  $\psi^r(t), r = 1, \dots, R$ . The algorithm is described, for example, in references [2,16,17]. As with any Monte Carlo method, the results are obtained through estimation from the sample of realizations. They are laden with a statistical error, which becomes smaller when the sample size  $R$  is increased.

## B. Time consumption

Let us denote by  $N$  the number of complex variables which are used for the numerical representation of the wave-function, that is, the number of basis states. The number of complex variables to represent the density matrix is then  $N^2/2$ .

In the case of the density matrix equation (DME), the part of the numerical integration routine that dominates the CPU time consumption is the calculation of the right-hand side of Eq. (1). One such calculation requires, for large enough  $N$ , an amount of CPU time proportional to a power of  $N$ , and the CPU time needed to integrate the density matrix over a given physical time interval is, to leading order in  $N$ ,

$$T_{\text{DME}} = k_1 s_1(N) N^\beta. \quad (4)$$

Here,  $s_1(N)$  is the number of times the right-hand side of Eq. (1) has to be evaluated.  $k_1$  and  $\beta$  depend on the type of the specific problem, but not on  $N$ . Besides,  $k_1$  depends on the particular implementation on a computer. Analogously, in many examples the time-critical part of the stochastic simulation (StS) is the calculation of the generator  $G(\psi)$ , and the CPU time required for the simulation is

$$T_{\text{StS}} = k_2 R(N) s_2(N) N^\alpha. \quad (5)$$

$R(N)$  is the number of realizations of the process that are generated to treat the system of size  $N$ ,  $s_2(N)$  is the number of evaluations of  $G(\psi)$  for one realization, and  $k_2$  is analogous to  $k_1$ .

In many situations,  $s_1(N)$  and  $s_2(N)$  will be roughly equal. Provided that similar numerical integration routines are used, this is the case if the smallest time scale of the dynamics of the stochastic wave-function is about equal to that of the density matrix. Since we want to separate the effects of system-size from dynamical phenomena, this case is the one of interest for this article, and the presented example illustrates that case.

Let us briefly note that there are also situations where  $s_1(N)$  and  $s_2(N)$  are quite different. In general their ratio might depend on  $N$  and they do not necessarily grow in the same way with the physical time over which the

system is studied. Consider the case where the time scale of the dynamics of a *single* realization of the stochastic process varies, during its temporal evolution, in a wide range, as for example, in laser cooling [18]. The simulation of one realization will then contain stretches with very long time steps, interrupted by phases of more rapid development and short time steps. The integrator of a density matrix equation, on the other side, which describes the dynamics of the whole ensemble, must always adapt to the short time scale. Clearly, in such cases the stochastic wave-function method is the preferred choice.

Independent of the specific form of the Hamiltonian  $H_S$ , the number of floating point operations to calculate the right-hand side of Eq. (1) and to calculate  $G(\psi)$  differ by about a factor  $N$ , and one expects

$$\beta \approx \alpha + 1. \quad (6)$$

This relation will be verified in the example of section III.

The crucial quantity for the relative performance is therefore the number of realizations  $R(N)$ . If it grows with  $N$  slower than linearly, then, regardless of the values of the factors  $k_1$  and  $k_2$ , the stochastic simulation will eventually be always faster for large systems, i. e., large  $N$ . In fact, as we shall see in Section III,  $R(N)$  can in many cases be chosen to be independent, or even a decreasing function of  $N$ .

The sample size  $R(N)$  is of course closely related to the statistical error of the estimated results. Consequently,  $R(N)$  is selected according to the desired accuracy of the results. The more accurate the results are supposed to be, the larger an  $R(N)$  we have to choose. A practical prescription for the tolerable statistical error may, for instance, be: "estimate the expectation value of the energy with a relative error of 1 %", or: "calculate the density matrix with a precision of better than  $10^{-4}$  in each of its elements". A meaningful comparison between the two methods on a general level is only possible if the behaviour of  $R(N)$  has general properties that are independent on the particular choice of prescription used, as well as on particularities of the system under study. In the following we shall see that this is indeed the case.

An unbiased and consistent estimator for the expectation value  $E_t[B]$  of an observable  $B$  (cf. Eq. (3)) is provided by the sample average,

$$\hat{B}_t = \frac{1}{R} \sum_{r=1}^R \langle \psi^r(t) | B | \psi^r(t) \rangle, \quad (7)$$

where  $\psi^r$  is the  $r$ -th realization generated by the algorithm, and  $R$  is the total number of independent realizations. Here and in the following, the hat denotes an estimator for the quantity underneath. The statistical error in the estimation can be measured by the square root of the variance of  $\hat{B}_t$ ,

$$\sigma_B := \sqrt{\text{Var}(\hat{B}_t)}. \quad (8)$$

The argument  $t$  stands for a given, fixed time, usually the end of the simulation. Since, from Eq. (7)

$$\text{Var}(\hat{B}_t) = \frac{1}{R} \text{Var}(\langle \psi(t) | B | \psi(t) \rangle), \quad (9)$$

$\sigma_B$  decreases proportionally to  $1/\sqrt{R}$ . The statistical error  $\sigma_B$  needs itself to be estimated from the sample of realizations, and an estimator  $\hat{\sigma}_B$  is constructed by employing Eq. (9), with the sample variance on the right-hand side.  $\hat{\sigma}_B$  is also often called the standard error of the mean.

The equation

$$\sigma_B^2 = \frac{\lambda_B(N)}{R} \quad (10)$$

defines a factor  $\lambda_B(N)$  that takes into account the dependence of the statistical error on the observable  $B$  and on the system size  $N$ , but does *not* depend on the sample size  $R$ . Using a sufficiently large sample of realizations,  $\lambda_B(N)$  can be determined by fitting Eq. (10) to the simulated data. Then, Eq. (10) can be solved for  $R$ ,

$$R \equiv R_B(N) = \frac{\lambda_B(N)}{\sigma_B^2}. \quad (11)$$

This is the number of realizations that is necessary to achieve an accuracy of  $\sigma_B$  for observable  $B$  and system size  $N$ .

In the example of section III,  $\lambda_B(N)$  is determined for various observables  $B$ . If  $\lambda_B(N)$  varies as a power of the system size,  $\lambda_B(N) \sim N^{-x}$ , the following classification can be made [19]:

1. If  $x = 1$ , the observable  $B$  is strongly self-averaging.
2. If  $0 < x < 1$ , the observable  $B$  is self-averaging.
3. If  $x = 0$ , the observable  $B$  is not self-averaging.

Concluding the general considerations, we can write Eqs. (4) and (5) in a more succinct form

$$\begin{aligned} T_{\text{DME}} &= k_1 N^{\alpha+1} \\ T_{\text{StS}} &= k_2 N^{\alpha-x}. \end{aligned}$$

Here we have assumed that the numbers of steps  $s_1$  and  $s_2$  are roughly equal and can be absorbed into the constants  $\alpha$ ,  $k_1$  and  $k_2$ . The performance of the stochastic wave-function method versus that of density matrix integration can be measured by the difference between the exponents, which is 1 in the non-self-averaging ( $x = 0$ ) and 2 in the strongly self-averaging case ( $x = 1$ ).

### III. SIMULATION

In this section the general considerations of Sec. II will be confirmed by means of numerical investigations of a non-trivial example, the excitation of molecular vibrations by short laser pulses in a dissipative environment.

#### A. Stochastic wave-function method

First, let us repeat very briefly some basic features of the stochastic wave-function method as far as they are necessary to understand the simulation. A piecewise deterministic stochastic process [20] is completely specified by the following quantities [14]:

1. The non-linear operator  $G$  that induces the norm-conserving deterministic flow according to

$$\partial\psi/\partial t = -\frac{i}{\hbar}G(\psi).$$

2. A set of jump operators  $A_\nu$ . The index  $\nu$  counts over the different possible jumps. The  $\nu$ -th jump is given by

$$\psi \rightarrow \frac{A_\nu \psi}{\|A_\nu \psi\|}.$$

3. A set of jump rates  $\gamma_\nu$ . At each time  $t$ , the probability for jump  $\nu$  to occur in the next time interval  $dt$  is

$$P(\text{jump } \nu \text{ within } [t, t+dt]) = \gamma_\nu \|A_\nu \psi(t)\| dt.$$

In the context of Markovian open quantum systems, these quantities are not fully independent: Instead of  $G$ , equivalently a linear, non-Hermitian operator

$$\tilde{H} = H_S - \frac{i\hbar}{2} \sum_\nu \gamma_\nu A_\nu^\dagger A_\nu, \quad (12)$$

and an unnormalized wave-function  $\tilde{\psi}$  can be used that obeys  $\partial\tilde{\psi}/\partial t = -i\tilde{H}\tilde{\psi}/\hbar$ . If the initial condition  $\psi(t_0) = \tilde{\psi}(t_0)$  is fulfilled, then the two wave-functions are related by  $\psi(t) = \tilde{\psi}(t)/\|\tilde{\psi}(t)\|$ .  $H_S$  is the Hamiltonian of the free system. Note that in the example of Section III B, the operators  $H_S$ ,  $\tilde{H}$  and  $G$  are explicitly time-dependent.

A further important quantity is the random waiting time  $\tau$  until the next jump occurs, given that the system is in a state  $\psi$  at time  $t$ . The cumulative distribution function of  $\tau$  can be shown to be [16]

$$F(\tau) = 1 - \left\| \tilde{\psi}(t + \tau) \right\|^2, \quad (13)$$

with the initial condition  $\tilde{\psi}(t) = \psi$ . This relation between the distribution of the waiting time and the norm of  $\tilde{\psi}$  is employed in the Monte Carlo generation of the waiting time.

The relation of the stochastic wave-function to the density operator is

$$\rho(t) = \int |\psi\rangle\langle\psi| P[\psi, t] D\psi D\psi^*, \quad (14)$$

i. e., the density matrix is the covariance matrix of the stochastic process  $\psi$ . In particular, expectation values of the kind (3) can equivalently be expressed as

$$E_t[B] = \text{Tr}\{B\rho(t)\}. \quad (15)$$

## B. Example: The damped driven Morse oscillator

The concept of laser control of chemical reactions by means of selective excitation of molecular vibrational states has received considerable interest in recent years [21]. In the simplest case, one might consider a single molecular degree of freedom within a single electronic potential energy surface:

$$H_M = \frac{1}{2m}p^2 + V(q). \quad (16)$$

For  $V(q)$ , consider the Morse potential

$$V(q) = D\{1 - \exp[-b(q - q_{eq})]\}^2.$$

With an appropriate choice of the parameters  $D$ ,  $b$  and  $q_{eq}$ , this model yields a fairly realistic description of, for example, the vibrational dynamics of the local O–H bond in the water molecule, or of the HF molecule [22–25]. Representing the interaction with the laser field semiclassically in dipole approximation, the interaction term is

$$H_L(t) = \mu q F_0 s(t) \sin(\omega_L t). \quad (17)$$

Here,  $\mu q$  is the relevant component of the molecular dipole moment,  $F_0$  is the maximum field strength and  $s(t)$  is the envelope of the laser pulse, or of a series of pulses. To be specific, we take

$$s(t) = \sin^2\left(\frac{\pi t}{t_p}\right).$$

In the language of Sec. II A, the ‘system’ is the non-dissipative driven Morse oscillator, and is represented by the Hamiltonian

$$H_S(t) = H_M + H_L(t). \quad (18)$$

A description based on the time-dependent Schrödinger equation with Hamiltonian  $H_S(t)$  applies for isolated polar bonds interacting solely with the laser pulse, i. e., for small molecules in a dilute gas. If the dynamics is restricted to bound states, a straightforward numerical approach consists in the numerical integration of the time-dependent Schrödinger equation in the energy eigenbasis of  $H_M$ . Selective excitation of a given target state with probabilities arbitrarily close to unity can be achieved by suitable choice of the laser pulse parameters  $F_0$  and  $t_p$  [26,27]. A good theoretical understanding of the mechanisms involved, as well as a simple criterion for optimal pulse design, is provided by representing the dynamics in a time-dependent comoving Floquet basis [24,25].

Inclusion of dissipative contributions to the dynamics is necessary if the molecule under consideration is embedded in a solid or dissolved in a liquid. Environment induced relaxation and dephasing have a significant effect on the excitation mechanism. In particular, it seems

no longer possible to achieve a selectivity as perfect as in the isolated case [28].

Within the formalism of the stochastic wave-function method, the dissipative part of the dynamics is described by specifying a set of jump operators, together with their respective jump rates. The present investigations are restricted to the case where the dynamics is well confined in the subspace  $\mathcal{H}$  of bound states of the Morse oscillator. The number of bound states is [29]

$$N = \text{int}\left(\frac{\sqrt{2mD}}{\hbar b} + \frac{1}{2}\right), \quad (19)$$

and the energy spectrum of  $H_M$  is given by

$$E_k = \sqrt{\frac{2D}{m}}\hbar b\left(k + \frac{1}{2}\right) - \frac{\hbar^2 b^2}{2m}\left(k + \frac{1}{2}\right)^2 \quad (20)$$

for  $k = 0, 1, \dots, N-1$ . For the jump operators, we chose a basis of the space of linear operators in  $\mathcal{H}$ ,

$$A_{jk} = |j\rangle\langle k| \quad j, k = 0, 1, \dots, N-1, \quad (21)$$

where  $|j\rangle$  is the eigenstate that belongs to  $E_j$ . The index pair  $(j, k)$  now plays the role of the index  $\nu$  in the general formalism of section III A. The operators  $A_{jk}$  are eigenoperators of  $H_M$ :

$$[H_M, A_{jk}] = (E_j - E_k)A_{jk}. \quad (22)$$

The effect of the jump operator  $A_{jk}$  on the system wavefunction may be interpreted as the transition which belongs to the emission or absorption of a vibration quantum of energy  $|E_j - E_k|$ . If we assume that the environmental degrees of freedom have a flat spectral density in the frequency range of interest and obey a thermal distribution, that the interaction is proportional to the system’s dipole moment, and that the relevant processes in the system-environment interaction are spontaneous emission as well as induced absorption and emission of vibration quanta, the jump rates are

$$\gamma_{jk} = \kappa |\langle j | q - q_{eq} | k \rangle|^2 \times \begin{cases} \bar{n}(\omega_{jk}) + 1, & \text{if } \omega_{jk} > 0 \\ 0, & \text{if } \omega_{jk} = 0 \\ \bar{n}(\omega_{jk}), & \text{if } \omega_{jk} < 0 \end{cases} \quad (23)$$

where

$$\hbar\omega_{jk} = E_k - E_j,$$

$\bar{n}(\omega_{jk})$  is the thermal distribution

$$\bar{n}(\omega_{jk}) = (e^{\hbar\omega_{jk}/k_B T} - 1)^{-1},$$

and  $\kappa$  is a constant of dimension  $(\text{time})^{-1}(\text{length})^{-2}$  that characterizes the strength of the system-environment coupling. Inserting Eq. (21) into Eq. (12), we find

that the deterministic part of the wave-function dynamics is governed by

$$\tilde{H}(t) = H_S(t) - \frac{i\hbar}{2} \sum_{j,k} \gamma_{jk} |k\rangle\langle k|.$$

The stochastic process, as well as the density matrix equation for the damped driven Morse oscillator are now completely specified. Numerical calculations have to be performed in a specific basis, for which we chose the (bound) eigenstates  $|j\rangle$  of  $H_M$ . The equation for  $\tilde{\psi}$  in the energy representation is

$$\frac{d}{dt} \tilde{\psi}_j = -\frac{i}{\hbar} \left( E_j \tilde{\psi}_j - f(t) \sum_{k=0}^{N-1} Q_{jk} \tilde{\psi}_k \right) - \frac{1}{2} \Gamma_j \tilde{\psi}_j. \quad (24)$$

Here,  $f(t)$  is the time-dependent external force (cf. Eq. (17))

$$f(t) = \mu F_0 s(t) \sin(\omega_L t),$$

and  $Q_{jk}$  are the matrix elements of the dipole operator,

$$Q_{jk} = \langle j | q - q_{eq} | k \rangle.$$

The matrix  $(Q_{jk})$  is real and symmetric.  $\Gamma_j$  is the total rate of all jumps away from  $|j\rangle$ ,

$$\Gamma_j = \sum_{m=0}^{N-1} \gamma_{mj}. \quad (25)$$

Inserting Eqs. (18) and (21) into Eq. (1), the density matrix equation in the energy representation takes the form

$$\begin{aligned} \frac{d\rho_{jk}}{dt} = & -\frac{i}{\hbar} (E_j - E_k) \rho_{jk} - \frac{i}{\hbar} f(t) \sum_l (Q_{jl} \rho_{lk} - Q_{lk} \rho_{jl}) \\ & + \delta_{jk} \left( \sum_l \gamma_{jl} \rho_{ll} \right) - \frac{1}{2} (\Gamma_j + \Gamma_k) \rho_{jk}. \end{aligned} \quad (26)$$

The choice of the simulation parameters was based on the physical model of a HF molecule driven by a laser pulse [25] and is shown in Table I. For simplicity, the initial condition was assumed to be the pure ground state  $|0\rangle$  of the Morse oscillator. Thus the initial probability density and the initial density matrix were

$$\begin{aligned} P[\psi, t = 0] &= \frac{1}{2\pi} \int_0^{2\pi} d\varphi \delta[\psi - e^{i\varphi} |0\rangle], \\ \rho(t = 0) &= |0\rangle\langle 0|, \end{aligned}$$

where  $\delta[\cdot]$  is the Dirac functional. Using these parameters, the number of bound states is  $N = 24$ , and for the non-dissipative oscillator (i.e.,  $\kappa = 0$  in Eq. (23)), a nearly 100 % population of the fifth excited state can be achieved.

In order to study the effect of the system size on the time consumption of the numerical routines, a series of similar oscillators with varying number  $N$  of bound states was investigated. The parameters of these oscillators were defined as follows. Solving Eq. (19) for  $b$ ,

$$b = \sqrt{2mD/\hbar N}$$

and fixing  $m$  and  $D$  to their values given in Table I,  $b$  is a function of  $N$ . The system size  $N$  was varied in the range  $N = 12, \dots, 78$ . In order to not just blow up the number of states, with the actual dynamics always staying in the same number of low-lying states, it is necessary to appropriately scale the driving field as well. To this end, let us define a target state  $|j^*\rangle$ ,

$$j^* = \text{int} \left( \frac{N}{5} + \frac{1}{2} \right),$$

and tune the laser frequency to be

$$\hbar\omega_L = \frac{E_{j^*} - E_0}{j^*}.$$

The laser amplitude  $F_0$ , the pulse length  $t_p$  and the effective charge  $\mu$  were kept fixed at the values specified in Table I.

The strength of the environment coupling is most conveniently expressed via the mean lifetime of a certain excited state [28],

$$\tau_{j^*} = (\Gamma_{j^*})^{-1},$$

with  $\Gamma_{j^*}$  as defined in Eq. (25). Specifying  $\tau_{j^*}$  is equivalent to specifying  $\kappa$ . The two combinations of environment parameters that were used in the simulations are displayed in Table II. Combination A corresponds to the parameters used in Ref. [28].

### C. Simulation results

The central part of the simulation programs is the numerical integration of Eqs. (24) and (26). We used the same Runge-Kutta procedure for both (`rkqc` and `odeint` from Ref. [30]).

Fig. 1 shows the occupation probabilities  $P_{0 \rightarrow k}(t) \equiv \rho_{kk}(t)$  of the oscillator eigenstates versus time resulting from the action of the laser pulse. In the non-dissipative case ( $\kappa = 0$ ), nearly 100 % selective excitation of the fifth eigenstate is achieved with the applied optimal pulse. Dissipation (parameter combination A) results in a broad distribution of the occupation probability over several excited states.

Now let us turn to the comparison between stochastic simulation algorithm and the integration of the density matrix equation. The first thing to do is, of course, to verify that both methods do indeed yield the same

results. Because of Eq. (15), all expectation values estimated from stochastic simulations should be equal, within the statistical error bars, to those calculated from the density matrix. Moreover, with increasing sample size, the simulation results should converge to the density matrix results. This is illustrated in Fig. 2. The lowest curve shows the squared difference

$$\delta_H = \left( \hat{H}_t - E_t[H_M] \right)^2 \quad (27)$$

between  $E_t[H_M] \equiv \text{Tr}\{H_M \rho(t)\}$ , the expectation value of the oscillator energy at time  $t = t_p$  obtained from integrating the density matrix equation, and  $\hat{H}_t$ , the value estimated from a sample of realizations of the stochastic process.  $\delta_H$  is plotted as a function of the sample size. To obtain Fig. 2, 100 subsamples of varying size were randomly drawn from a pool of a total 2000 realizations that were generated by the simulation program. For Fig. 2 environment parameter combination A was used; the plot for combination B is similar. The upper two curves show the maximum of the squared differences between the diagonal and off-diagonal elements of the two density matrices,

$$\delta_{\text{diag}} = \max_k (\hat{\rho}_{kk} - \rho_{kk})^2 \quad (28)$$

$$\delta_{\text{off-diag}} = \max_{j \neq k} (\hat{\rho}_{jk} - \rho_{jk})^2, \quad (29)$$

where  $\hat{\rho}_{jk}$  is the estimator for the matrix element  $\langle j | \rho | k \rangle$ :

$$\hat{\rho}_{jk} = \frac{1}{R} \sum_{r=1}^R \langle j | \psi^r(t) \rangle \langle \psi^r(t) | k \rangle. \quad (30)$$

Clearly,  $\delta_{\text{diag}}$  and  $\delta_{\text{off-diag}}$  decrease with sample size, and systematic errors (induced, e.g., by round-off errors or by imperfections in the random number generator) are found to be negligible.

The next issue to look at are the exponents  $\alpha$  and  $\beta$  which were introduced in Section II B, cf. Eqs. (4) and (5). Fig. 3 shows the CPU time per time step of the numerical integrator as a function of the system size  $N$ . For Fig. 3 it makes no difference whether the environment parameter combination A or B is used. Measuring the slope of the lines, we obtained

$$\beta = 3.0 \pm 0.1, \quad \alpha = 2.0 \pm 0.1,$$

which confirms Eq. (6). These exponents can be easily understood: in the case of the stochastic simulation, the most time-consuming part is the multiplication of  $\tilde{\psi}$  with the dipole matrix  $Q$  (cf. Eq. (24)), which requires  $O(N^2)$  floating point operations. Analogously, for the density matrix integration, the calculation of the right-hand side of Eq. (26) for all  $j$  and  $k$  involves  $O(N^3)$  floating point operations.

Fig. 4 displays the number of integrator steps  $s_1$  and  $s_2$  that are necessary to calculate a whole pulse. As we

can see  $s_1$  and  $s_2$  increase with  $N$ , but remain roughly equal. Their increase is due to particular properties of the presented example. The systems of differential equations which have to be solved for the density matrix calculation and for the stochastic simulation both become stiffer with increasing  $N$ . In particular, the ratio between the highest and the lowest eigenenergy of the oscillator grows about linearly with increasing  $N$ .

In order to investigate the behaviour of  $R(N)$ , the number of Monte Carlo realizations that have to be generated to treat a system of size  $N$ , it is necessary to look at the standard error of various observables (see Section II B). An obvious choice for the observable of interest is the oscillator energy  $H_M$ , whose standard error we call  $\hat{\sigma}_H$ . More generally, it is possible to consider elements  $\hat{\rho}_{jk}$  of the density matrix (cf. Eq. (30)). Denoting their standard error by  $\hat{\sigma}_{jk}$ , we can define

$$\hat{\sigma}_{\text{diag}} = \max_k \hat{\sigma}_{kk}, \quad (31)$$

$$\hat{\sigma}_{\text{off-diag}} = \max_{j \neq k} \hat{\sigma}_{jk}, \quad (32)$$

the maximum standard error for diagonal and off-diagonal elements, respectively. Fig. 5 shows  $\hat{\sigma}_{\text{diag}}$ ,  $\hat{\sigma}_{\text{off-diag}}$  and  $\hat{\sigma}_H$  as a function of the sample size  $R$ . Fig. 5 was obtained, like Fig. 2, by randomly drawing 100 subsamples of varying size from a pool of a total 2000 realizations. After verifying that the curves are statistically consistent with straight lines of slope  $-1$ , the parameters  $\lambda_{\text{diag}}$ ,  $\lambda_{\text{off-diag}}$  and  $\lambda_H$  can be found according to Eq. (10) by linear regression on the logarithmic data.

In this manner, the  $\lambda$ -parameters were determined from a series of simulations with varying  $N$  and for the two different environment parameter sets. The results are presented in Fig. 6. Up to statistical fluctuations,  $\lambda(N)$  and therefore  $R(N)$  is a non-increasing function of  $N$ . Therefore, in order to achieve a constant statistical error in the simulation results when the system size  $N$  is increased, the number of realizations need not be increased. It follows that the stochastic simulation will eventually, for large system size, be always faster than solving the density matrix equation. This is the main result of the presented study.

This result is exemplified in Fig. 7: The plots show the CPU times needed to integrate the density matrix equation ( $\Delta$ ) and to generate as many realizations of the stochastic process ( $\diamond$ ) as are necessary to obtain a standard error of the mean of the oscillator energy  $\sigma_H = 4 \cdot 10^{-3}$ . The number of realizations  $R$  was calculated according to Eq. (11). According to Fig. 6c, we chose  $\lambda_H(N) = 10^{-3}$  independently of  $N$ . The curves follow different power laws and at some point  $N_0$  they intersect. In the present example,  $N_0 \approx 35$  for the weak dissipation case and  $N_0 \approx 55$  for the case of strong dissipation. Above  $N_0$ , the stochastic simulation is faster.

#### IV. CONCLUSION

It is commonplace that Monte Carlo algorithms are the only way to study very high-dimensional systems, for which exact deterministic calculations are beyond the capacity of any computing machinery. On the other hand, a deterministic method may be preferred for small systems. In this study, using a non-trivial example of intermediate size, the dependence of the CPU time consumption on the system size has been investigated for the quantum stochastic wave-function method and for the numerical integration of the corresponding density matrix equation. It has been possible to analyze the CPU time consumption in terms of simple power laws. The main result of the numerical study is that the CPU time for the density matrix integration  $T_{\text{DME}}$  and the time for the stochastic wave-function simulation  $T_{\text{StS}}$  scale with the system size  $N$  as

$$\begin{aligned} T_{\text{DME}} &\sim N^3, \\ T_{\text{StS}} &\sim N^2. \end{aligned} \quad (33)$$

Although the numerical study was performed on a specific example, the considerations made in Section II B are far more general. In particular, whereas the absolute values of the exponents in Eqs. (33) depend on specific properties of the system under study, their difference is of more general significance. Under general conditions, the exponent in the expression for  $T_{\text{DME}}$  is expected to be larger by 1 to 2 than the exponent of  $T_{\text{StS}}$ .

For a systematic comparison of the performance of the stochastic wave-function method and density matrix integration, the following two main points had to be taken into account.

First, one has to determine the number  $R$  of realizations of the stochastic process that have to be generated in the simulation. This number is related to the type of the observable under interest as well as to the desired accuracy. Quantitatively, this relation may be expressed in the form

$$R \sim \frac{N^{-x}}{\sigma^2}, \quad (34)$$

where  $\sigma$  is the desired standard error of the mean and  $x$  is an exponent that varies between 0 and 1, depending on the so-called self-averaging property [19] of the observable. Note that Eqs. (33) correspond to a non-self-averaging observable; the difference in the exponents would be even larger in the self-averaging case. An example of a self-averaging observable is the position operator of a particle when working in position representation.

Second, we analyzed the time consumptions in terms of “CPU time per integrator step” times “number of integrator steps”, and both factors have to be investigated separately. The present study focuses on the first factor and assumes that the second is roughly equal for the two numerical methods. However, if the second factor

is different, one can generally expect -as we discussed in Section II B- that the advantage will be with the stochastic wave-function method.

Due to the recent developments in computer technology, there is currently a trend in scientific computing towards parallel computing. The quantities  $T_{\text{DME}}$  and  $T_{\text{StS}}$  that have been investigated above stand for the time that the programs run on a single processor. When comparing numerical algorithms that run on a parallel computer, other important criteria are speed-up and scalability. The speed-up is defined as the ratio between the wall-clock times needed to do the job on the single processor and on the parallel computer. Scalability means that the speed-up is close to the number of processors of the parallel machine, for a wide range of numbers of processors. This implies that little time is spent on communication and synchronization overhead. Whereas an efficient, scalable parallelization of the density matrix numerical integration appears to be a complicated task, the stochastic wave-function method is an intrinsically parallel and very well scalable algorithm: since the individual realizations are generated independently, the only communication needed is for the final averaging or archiving, and for parameter control. Load balancing means that the parallel program adapts to a heterogeneous network with processors of varying speed, whose load may vary in time because of a time-sharing operating system. If the total number of realizations to be generated is much larger than the number of processors, it is straightforward and easy to perform an efficient load balancing. An implementation of the stochastic wave-function method on an IBM RS/6000 cluster with 7 processors, using a message passing library (MPI) that realizes all these features was used to generate the stochastic simulations presented in this article.

#### ACKNOWLEDGEMENT

One of us (W.H.) gratefully acknowledges financial support by the Deutsche Forschungsgemeinschaft within the Schwerpunktprogramm *Zeitabhängige Phänomene und Methoden in Quantensystemen der Physik und Chemie*.

---

- [1] J. Dalibard, Y. Castin, and K. Mølmer, Phys. Rev. Lett. **68**, 580 (1992).
- [2] K. Mølmer, Y. Castin, and J. Dalibard, J. Opt. Soc. Am. B **10**, 524 (1993).
- [3] R. Dum, P. Zoller, and H. Ritsch, Phys. Rev. A **45**, 4879 (1992).
- [4] N. Gisin and I. C. Percival, J. Phys. A: Math. Gen. **25**, 5677 (1992).

[5] H. P. Breuer and F. Petruccione, Phys. Rev. A **55**, 3101 (1997).

[6] B. Wolfseder and W. Domcke, Chem. Phys. Lett. **235**, 370 (1995).

[7] Y. Castin and K. Mølmer, Phys. Rev. Lett. **74**, 3772 (1995).

[8] R. Zwanzig, J. Chem. Phys. **33**, 1338 (1960).

[9] F. Haake, in *Quantum Statistics in Optics and Solid State Physics, Springer Tracts in Modern Physics 66* (Springer-Verlag, Berlin, 1973).

[10] W. Louisell, *Quantum Statistical Properties of Radiation* (Wiley, New York, 1990).

[11] R. Bausch, Z. Phys. **193**, 246 (1966).

[12] H. Haken, in *Encyclopedia of Physics* (Springer-Verlag, Berlin, 1970), Vol. XXV/2c.

[13] C. W. Gardiner, *Quantum Noise* (Springer-Verlag, Berlin, 1991).

[14] H. P. Breuer and F. Petruccione, Phys. Rev. E **51**, 4041 (1995).

[15] H. P. Breuer and F. Petruccione, Phys. Rev. Lett. **74**, 3788 (1995).

[16] H. P. Breuer and F. Petruccione, Phys. Rev. E **52**, 428 (1995).

[17] C. W. Gardiner, A. S. Parkins, and P. Zoller, Phys. Rev. A **46**, 4363 (1992).

[18] F. Bardou *et al.*, Phys. Rev. Lett. **72**, 203 (1994).

[19] A. M. Ferrenberg, D. P. Landau, and K. Binder, J. Stat. Phys. **63**, 867 (1991).

[20] M. H. A. Davis, *Markov Models and Optimization* (Chapman & Hall, London, 1993).

[21] *Femtosecond Chemistry*, edited by J. Manz and L. Wöste (VCH, Weinheim, New York, 1995).

[22] W. Jakubetz, J. Manz, and V. Mohan, J. Chem. Phys. **90**, 3686 (1989).

[23] W. Jakubetz, B. Just, J. Manz, and H. J. Schreier, J. Phys. Chem. **94**, 2294 (1990).

[24] H. P. Breuer, K. Dietz, and M. Holthaus, J. Phys. B: At. Mol. Opt. Phys. **24**, 1343 (1991).

[25] H. P. Breuer, K. Dietz, and M. Holthaus, Phys. Rev. A **45**, 550 (1992).

[26] G. K. Paramonov, V. A. Savva, and A. M. Samson, Infrared Phys. **25**, 201 (1985).

[27] Z. E. Dolya, N. B. Nazarova, G. K. Paramonov, and V. A. Savva, Chem. Phys. Lett. **145**, 499 (1988).

[28] D. Malzahn and V. May, Chem. Phys. **197**, 205 (1995).

[29] D. ter Haar, *Selected Problems in Quantum Mechanics* (Infosearch Ltd., London, 1964).

[30] W. H. Press, S. A. Teukolsky, W. T. Vetter, and B. P. Flannery, *Numerical Recipes in C* (Cambridge University Press, Cambridge, 1992).

Reduced Mass $m$	1744.805	$m_{el}$
Potential Depth $D$	0.22509	hartree
Morse Parameter $b$	1.1741	$a_0^{-1}$
Effective Charge $\mu$	0.3099	$q_{el}$
Laser Amplitude $F_0$	0.0431	hartree/( $q_{el}a_0$ )
Laser Frequency $\omega_L$	0.016489	hartree/ $\hbar$
Laser Pulse Length $t_p$	$100 \cdot 2\pi/\omega_L$	$\simeq 922$ fs

TABLE I. The simulation parameters of the Morse oscillator and the laser pulse. The Bohr radius  $a_0$  is  $5.29177 \cdot 10^{-11}$  m, 1 hartree is equivalent to  $4.35 \cdot 10^{-18}$  J.

	A	B
Temperature $T$	300 K	$\hbar\omega_L/k_B$
Mean lifetime of target state $\tau_{j^*}$	$0.5 t_p$	$0.01 t_p$

TABLE II. The two combinations of environment parameters that were employed in the simulations. Using combination A, the dynamics is dominated by its coherent part and there are only a few (about 2 on average) quantum jumps within the time of the pulse. With combination B the number of jumps is much larger, and dissipative effects are more dominant.

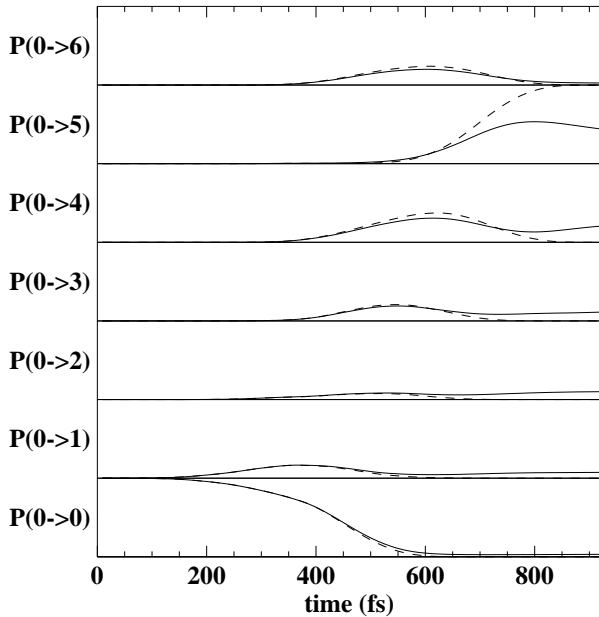


FIG. 1. The occupation probabilities  $P_{0 \rightarrow k}(t) \equiv \rho_{kk}(t)$  of the oscillator eigenstates versus time resulting from the action of the laser pulse. The oscillator parameters correspond to those of a HF molecule and are stated in the text. The dashed lines correspond to the non-dissipative situation, and show that with the applied optimal laser pulse, nearly perfect selective excitation of the fifth eigenstate is achieved. The solid lines show what happens when an environment coupling is present. The coupling strength is such that the mean lifetime of the fifth excited state,  $\tau_5$ , is half the pulse length (parameter combination A).

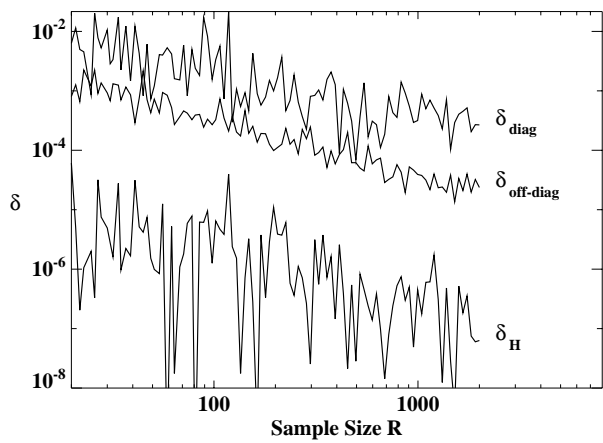


FIG. 2. The difference between quantities estimated from stochastic simulations and those obtained from integrating the density matrix equation as a function of the sample size  $R$ .  $\delta_H$ ,  $\delta_{\text{diag}}$  and  $\delta_{\text{off-diag}}$  are defined in Eqs. (27-29).

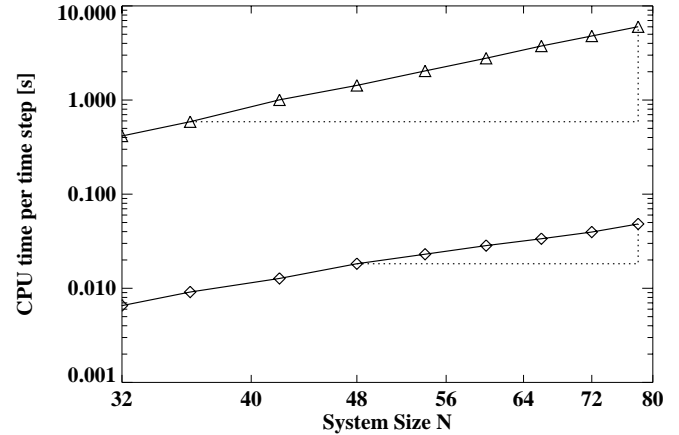


FIG. 3. The CPU time per step for the integration of the density matrix equation ( $\Delta$ ) and for the propagation of the wave vector  $\psi$  ( $\diamond$ ). The dotted lines indicate how the exponents  $\alpha$  and  $\beta$  were calculated from the slope; the continuous lines simply connect the data points.

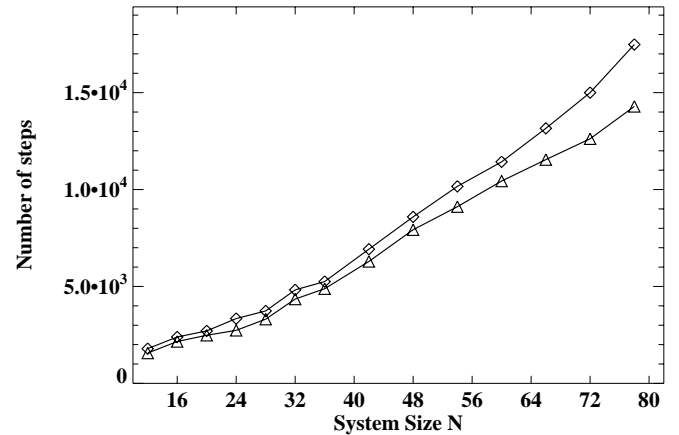


FIG. 4. The triangles ( $\Delta$ ) display  $s_1$ , the number of integrator steps to calculate one pulse using the density matrix equation. The diamonds ( $\diamond$ ) show  $s_2$ , the average number of steps to calculate one realization of the stochastic process. For this plot, environment parameter combination A was employed.

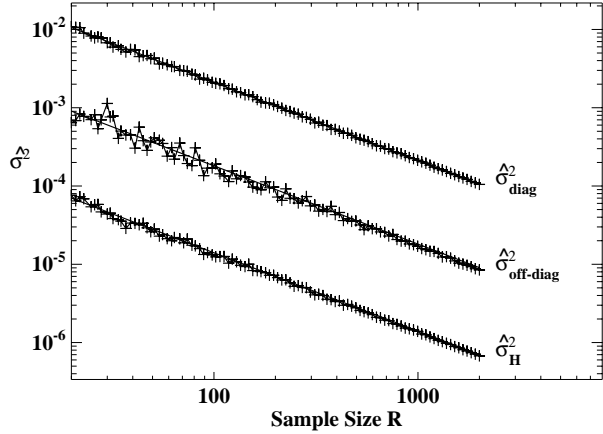


FIG. 5. The squared standard error of the mean of the oscillator energy ( $\hat{\sigma}_H^2$ ), the maximum squared standard error of the diagonal ( $\hat{\sigma}_{\text{diag}}^2$ ) and of the off-diagonal ( $\hat{\sigma}_{\text{off-diag}}^2$ ) elements of the estimated density matrix as functions of the sample size  $R$ . See also Eqs. (31) and (32). For this plot, the system size  $N$  was 24 and environment parameter combination A was employed. The plots for other system sizes and for environment parameter combination B look similar. All fitted straight lines have slope -1, and from their intersection with the  $y$ -axis at  $R = 1$  the parameters  $\lambda(N)$  were determined according to Eq. (10).

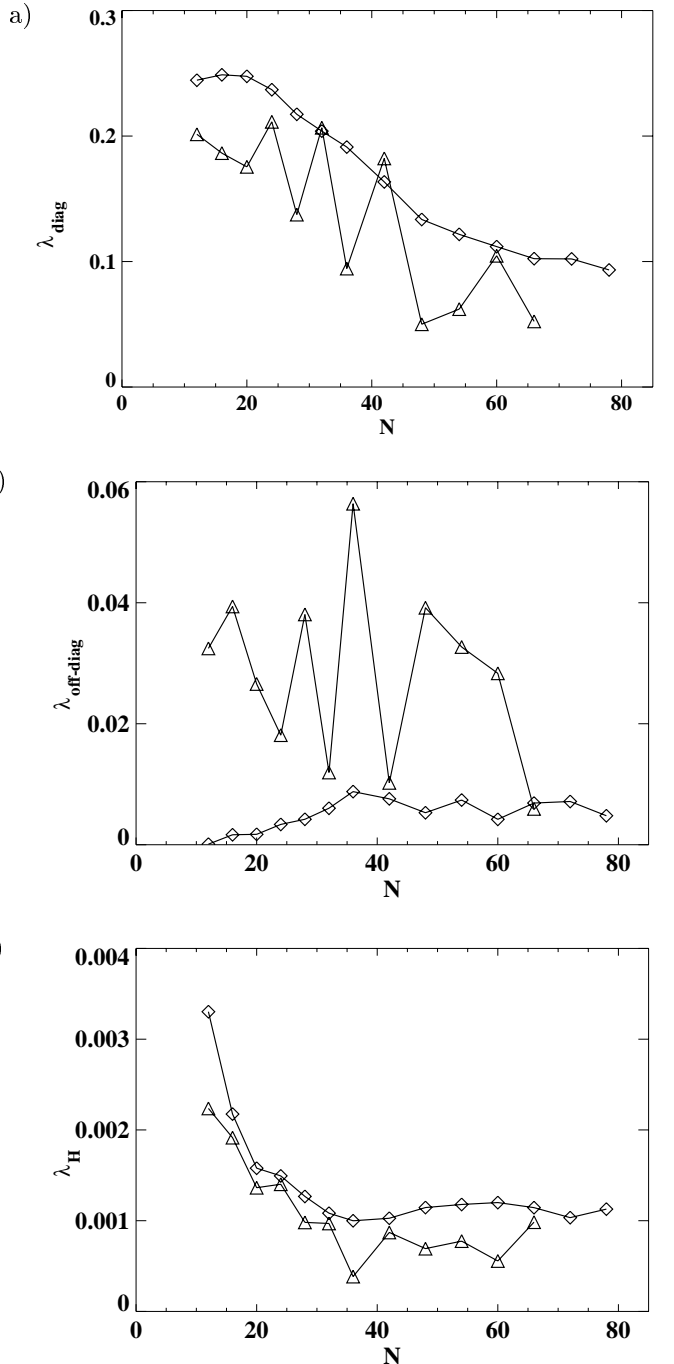


FIG. 6. The function  $\lambda_B(N)$  measures the self-averaging property of the observable  $B$ , cf. Eq. (10). The figure shows a)  $\lambda_{\text{diag}}$ , b)  $\lambda_{\text{off-diag}}$  and c)  $\lambda_H$ . These quantities were obtained from graphs like in Fig. 5 as described in the text. The triangles  $\Delta$  correspond to weak dissipation (environment parameter combination A), the diamonds  $\diamond$  to strong dissipation (combination B). From these plots we conclude that, in order to achieve a constant statistical error in the simulation results when the system size  $N$  is increased, the number of realizations need not be increased.

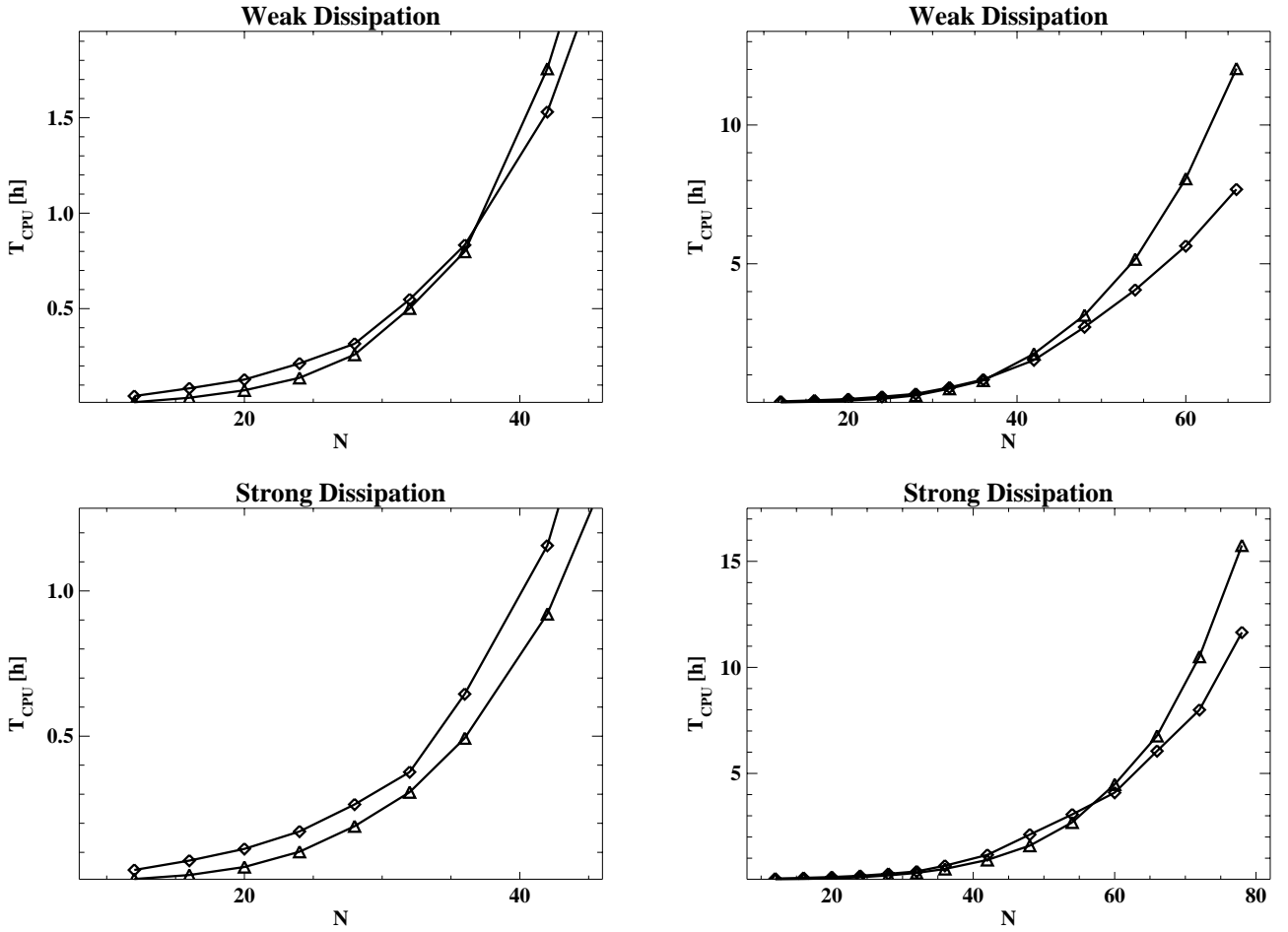


FIG. 7. CPU times needed to integrate the density matrix equation ( $T_{DME}$ ,  $\Delta$ ) and to generate as many realizations of the stochastic process ( $T_{sts}$ ,  $\diamond$ ) as are necessary to obtain a standard error of the mean of the oscillator energy  $\sigma_H = 4 \cdot 10^{-3}$ . The plots on the right-hand side cover the full variation of system size we investigated while the plots on the left side zoom in at lower  $N$ . The curves follow different power laws and at some point  $N_0$  they intersect. Above  $N_0$ , the stochastic simulation is faster.